

Chapter 5

Minimum Bias, Underlying Events and Multiple Interactions

Authors: Filippo Ambroglini, Paolo Bartalini, Livio Fanò, Lucia Garbini, Daniele Treleani

Revisors: Paolo Nason

5.1 Introduction

This chapter is sub-divided in four sections. The next section gives the definition of “min-bias” and “underlying event”. A brief review of the current status of the phenomenological studies and theoretical models is given in section 5.3. The measurement plan at the LHC is described in section 5.4, where the relevant observables sensitive to the examined processes are introduced by comparing different tunings of the most popular Monte Carlo models.

5.2 Definition of the physics processes

Events collected with a trigger that is not very restrictive are referred to as minimum bias events (MB). The total proton-proton cross section is the sum of the elastic cross section and the inelastic cross section. The inelastic cross section receives contributions from single and double diffraction. The remainder of the inelastic cross section is referred to as the “hard core” component. Minimum bias events typically contain some single and double diffraction as well as most of the “hard core” component of the inelastic cross section. The “hard core”

component does not always correspond to a “hard scattering”. Quite often the beam and target hadrons ooze through each other and fall apart without any “hard” collisions occurring in the event. At the Tevatron about 1% of min-bias events contain a jet with 10 GeV transverse energy. At the LHC we expect the fraction of MB events with a 10 GeV jet to increase by more than a factor of 10 from the Tevatron to about 12%. We expect about 1% of MB events at the LHC to contain a 20 GeV jet. Understanding and modeling the jet structure of MB events is crucial at the LHC because of the large amount of pile-up expected.

From an experimental point of view, in a hadron-hadron interaction with jets in the final state, the “underlying event” is all the activity accompanying the 2 hard scattered outgoing jets. It is impossible to separate these two components due to the lack of knowledge in modeling the underlying jet structure. Anyway one can use the topological structure of hadron-hadron collisions to define physics observables that are mostly sensitive to the underlying activity. The typical approach is to rely on particle and energy densities in η - ϕ regions that are well separated with respect to the high P_T objects (for example jets). In shower Monte Carlo model, the “underlying event” is a component of the process simulation that acts at the end of the showering and before the hadronization, in order to complete the process description taking into account soft components (hadronic remnants and multiple interaction).

Huge progress in the phenomenological study of the underlying event in jet events has been achieved by the CDF experiment at the Tevatron [18, 19], using the multiplicity and transverse momentum spectra of charged tracks in different regions of the azimuth-pseudorapidity space, defined with respect to the direction of the leading jet. Regions that receive energy flow contributions mostly by the underlying event have been identified. The CDF UE analysis showed that the density of particles in the UE in jet events is about a factor of two larger than the density of particles in a typical Minimum Bias (MB) collision. This effect, referred to as “pedestal effect”, is well reproduced only by varying impact parameters models with correlated parton-parton interactions. Simpler models seem to be ruled out. In general the most successful models predict an even more relevant difference between the MB and the UE activities at the LHC, with deep consequences on lepton and photon isolation, jet energy calibrations, etc.

5.3 The QCD models and the Multiple Parton Interaction concept

In the years '80, the evidence for Multiple Parton Interaction (MPI) phenomena in the high- P_T phenomenology of hadron colliders [1, 2, 3] suggested the extension of the same perturbative picture to the soft regime, giving rise to the

first implementation of the MPI processes in a QCD Monte Carlo model ⁴⁾.

These models turned out to be particularly adequate to describe the MB and the UE physics. In particular, the pedestal effect mentioned in sec. 1.2 can be explained partly¹ as an increased probability of multiple partonic interaction in case a hard collision has taken place (a hard scattering is more likely to be present in a small impact parameter collision, which thus implies more additional parton-parton interactions).

Examples of MPI models are implemented in the general purpose simulation programs PYTHIA ⁵⁾, HERWIG/JIMMY ⁶⁾ and SHERPA ⁷⁾. Other successful descriptions of UE and MB at hadron colliders are achieved by alternative approaches like PHOJET ⁸⁾, which was designed to describe rapidity gaps and diffractive physics (relying on both perturbative QCD and Dual Parton Models). The purely phenomenological UE and MB description available in HERWIG ⁹⁾ provides a very useful reference of a model not implementing multiple interactions. The most recent PYTHIA version ¹⁰⁾ adopts an optional alternative description of the colliding partons in terms of correlated multiparton distribution functions of flavours, colors and longitudinal momenta.

All these models have to be tested and tuned at the LHC, in particular for what concerns the energy dependent parameters.

5.3.1 The SPS and Tevatron legacies

The QCD models considered here are three different PYTHIA 6.4 Tunes (with 2 different MPI models) and HERWIG (without MPI) as reference. The relevant parameters of the different PYTHIA Tunes are summarized in table 5.1.

The main parameter of the PYTHIA tunes, $P_{T_{min}}$, is the minimum transverse momentum of the parton-parton collisions; it effectively controls the average number of parton-parton interactions, hence the average particle multiplicity. The studies reported in ¹¹⁾, considering a homogeneous sample of average charged multiplicity measurements at six different center-of-mass energies ($\sqrt{s} = 50, 200, 546, 630, 900$ and 1800 GeV) in the pseudo-rapidity region $|\eta| < 0.25$ ^{12, 13)}, show that the power law expressed in the following Equation:

$$P_{T_{min}}^{(s)} = P_{T_{min}}^{(s')} \left(\frac{s}{s'} \right)^\epsilon \quad (5.1)$$

holds for values of ϵ between $\simeq 0.08$ and $\simeq 0.10$ if post-HERA parton distribution functions are used.

¹A second important effect that can contribute to the pedestal is the increase in initial state radiation associated to the presence of a hard scattering

All the considered PYTHIA tunes adopt varying impact parameter models with a continuous turn-off of the cross section at $P_{T_{min}}$ and hadronic matter in the colliding hadrons described by two concentric Gaussian distributions¹⁵⁾. These models were initially developed to reproduce the UA5 MB charged multiplicity¹⁶⁾. The variations of the impact parameter introduce correlations between the MPI, giving rise to a charged multiplicity shape which is basically the convolution of several Poissonians. This can be clearly seen in Fig. 5.2.

All the considered PYTHIA tunes describe the basic Tevatron UE phenomenology in a reasonable way. One of the PYTHIA models is Tune DW²⁰⁾, a tune by R. Field which is similar to Tune A²¹⁾, reproducing also the CDF Run 1 Z-boson transverse momentum distribution²²⁾ Tune DWT²⁰⁾ is identical to Tune DW at the Tevatron (*i.e.*, 1.96 TeV), but uses the same MPI energy dependence parameter as the ATLAS tune²³⁾ ($\epsilon = 0.08$). Tune S0²⁴⁾ also adopts the same energy dependence parameter as the ATLAS tune, however, In contrast to DW and DWT, it does adopt the new PYTHIA multiple interaction framework.

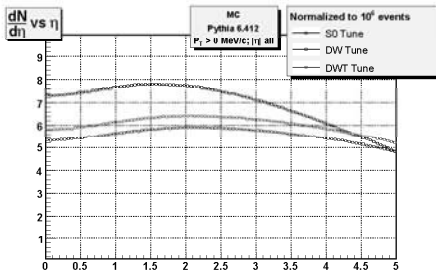


Figure 5.1: Charged particle density distribution, $dN_{chg}/d\eta$, for Minimum Bias events at LHC condition with PYTHIA6.412 and Tune DW, DWT and S0.

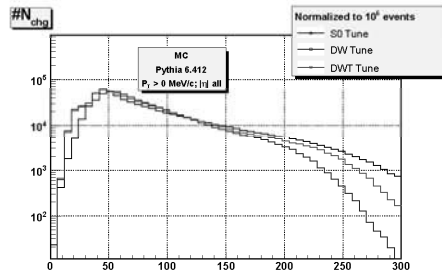


Figure 5.2: Charged particle distribution for Minimum Bias events at LHC condition with PYTHIA6.412 and Tune DW, DWT and S0.

5.4 The Measurement plan at the LHC

5.4.1 The Basic Minimum Bias Observables

One of the first results of LHC will be the measurement of the charged multiplicity and p_T spectrum in proton-proton collisions at $\sqrt{s} = 14$ TeV¹⁷⁾.

Parameter (PYTHIA v.6412+)	A	ATLAS	DW	DWT	S0
UE model MSTP(81)	1	1	1	1	21
UE infrared regularisation scale PARP(82)	2.0	1.8	1.9	1.9409	1.85
UE scaling power with \sqrt{s} PARP(90)	0.25	0.16	0.25	0.16	0.16
UE hadron transverse mass distribution MSTP(82)	4	4	4	4	5
UE parameter 1 PARP(83)	0.5	0.5	0.5	0.5	1.6
UE parameter 2 PARP(84)	0.4	0.5	0.4	0.4	n/a
UE total gg fraction PARP(86)	0.95	0.66	1.0	1.0	n/a
ISR infrared cutoff PARP(62)	1.0	1.0	1.25	1.25	(= PARP(82))
ISR renormalisation scale prefactor PARP(64)	1.0	1.0	0.2	0.2	1.0
ISR Q_{max}^2 factor PARP(67)	4.0	1.0	2.5	2.5	n/a
ISR infrared regularisation scheme MSTP(70)	n/a	n/a	n/a	n/a	2
ISR FSR off ISR scheme MSTP(72)	n/a	n/a	n/a	n/a	0
FSR model MSTJ(41)	2	2	2	2	(p_t - ordered)
FSR Λ_{QCD} PARJ(81)	0.29	0.29	0.29	0.29	0.14
BR colour scheme MSTP(89)	n/a	n/a	n/a	n/a	1
BR composite x enhancement factor PARP(79)	n/a	n/a	n/a	n/a	2
BR primordial k_T width $< k_T >$ PARP(91)	1.0	1.0	2.1	2.1	n/a
BR primordial k_T UV cutoff PARP(93)	5.0	5.0	15.0	15.0	5.0
CR model MSTP(95)	n/a	n/a	n/a	n/a	6
CR strength ξ_R PARP(78)	n/a	n/a	n/a	n/a	0.2
CR gg fraction (old model) PARP(85)	0.9	0.33	1.0	1.0	n/a

Table 5.1: Set of parameters defining the different versions of the PYTHIA 6.4 models adopted in this study. In all the configurations, the CTEQ5L parton distribution functions are considered. The parameters are subdivided into five main categories: UE (underlying event), ISR (initial state radiation), FSR (final state radiation), BR (beam remnants), and CR (colour reconnections). The UE reference energy for all models is PARP(89)=1800GeV. GeV unit is adopted if applicable.

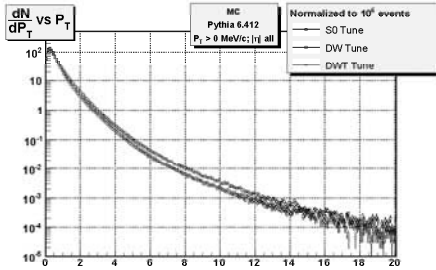


Figure 5.3: Charged particle density distribution, dN_{chg}/dP_t , for Minimum Bias events at LHC condition with PYTHIA6.412 and Tune DW, DWT and S0.

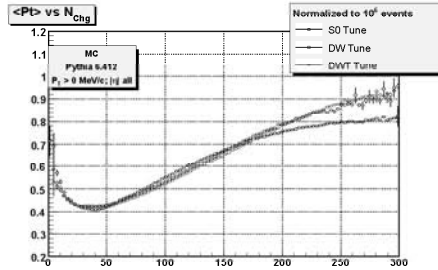


Figure 5.4: Average P_t as a function of chareg multiplicity, for Minimum Bias events at LHC condition with PYTHIA6.412 and Tune DW, DWT and S0.

The predictions of the considered PYTHIA tunes for these MB observables are reported in Fig. 5.1 and Fig. 5.3 respectively.

In Reference ¹³⁾ the energy dependence of $dN_{ch}/d\eta$ at $\eta = 0$ is fitted to older data using a linear and quadratic functions of $\ln(s)$. Using these fits to extrapolate at LHC energy would predict $dN_{ch}/d\eta = 6.11 \pm 0.29$ at $\eta = 0$ (to be compared with the predictions of the models given by the intercept of the y axis and the curves of Fig. 5.1).

5.4.2 The Underlying Event as Observed in Charged Jet Events

One can use the topological structure of hadron-hadron collisions to study the UE. Furthermore, this can be done by looking only at the outgoing charged particles ¹⁸⁾. Jets are constructed from the charged particles using a simple clustering algorithm and then the direction of the leading charged particle jet is used to isolate regions of the η - ϕ space that are sensitive to the UE. As illustrated in Fig. 5.5, the direction of the leading charged particle jet, $chjet1$, is used to define correlations in the azimuthal angle, $\Delta\phi$. The angle $\Delta\phi = \phi - \phi_{chjet1}$ is the relative azimuthal angle between a charged particle and the direction of $chjet1$.

The charged jet energy provide an indication of the energy scale of the event. Adopting the charged does allow to investigate the very low energy scale region (down to $P_T \rightarrow 0$ GeV/c) which is not accessible to the calorimetric jets. In other words, the charged jet does provide a better understanding of the systematic effects in the low P_T limit, that can be interpreted in terms of very

well understood quantities like the tracking efficiency and fake rate. Another big advantage of the measurement relying on the charged tracks is its intrinsic insensitiveness to the pile up effect as only the charged particles coming from the primary vertex are retained in the computation of the UE observables.

The “transverse” region is almost perpendicular to the plane of the hard 2-to-2 scattering and is therefore very sensitive to the UE. We restrict ourselves to charged particles in the central region $|\eta| < 2$ and consider two p_T thresholds, the nominal CMS cut $p_T > 0.9 \text{ GeV}/c$ and a lower threshold with $p_T > 0.5 \text{ GeV}/c$.

Ultimately we would like to disentangle the hard initial and final state radiation (*i.e.*, multijet production) from the beam-beam remnants and MPI components. This can be done by separating the various jet topologies. First one considers events with at least one jet and uses the leading jet direction to define the “transverse” region (referred to as “leading jet” events). Of course some of these “leading jet” events contain multijets that contribute to the activity in the “transverse” region. Next one considers “back-to-back” dijet events which are a subset of the “leading jet” events. The “transverse” region for the “back-to-back” dijet events contains much less hard initial and final state radiation and by comparing the two classes of events one can learn about gluon radiation as well as the beam-beam remnants and the MPI component. In this note we will only discuss the “leading jet” events.

The charged jet p_T range 0 to 200 GeV/c shown in Figs. 5.6 and 5.7 is quite interesting. The three versions of PYTHIA (with MPI) behave much differently than HERWIG (without MPI). Due to the MPI the PYTHIA tunes rise rapidly and then reach an approximately flat “plateau” region at $P_T(\text{chgjet1}) \approx 20 \text{ GeV}/c$. Then at $P_T(\text{chgjet1}) \approx 50 \text{ GeV}/c$ they begin to rise again due to initial and final state radiation which increases as the Q^2 scale of the hard scattering increases. The rise is more evident for the high p_T threshold $p_T > 0.9 \text{ GeV}/c$. HERWIG has considerably fewer particles in the “transverse” region and predicts a steady rise over this region resulting from initial and final state radiation.

Due to higher effective cut off in the Q^2 of the MPI, the Tune DW does achieve predictions which are around 25% below with respect to the DWT and S0 for what concerns both the particle and energy densities. Even with a modest statistics, at the LHC we will be able to distinguish between these two different trends reflecting different choices of the energy dependent parameters in multiple interactions.

The S0 tune predicts a larger charged particle density in the “transverse” region than Tune DWT for $p_T > 0.5 \text{ GeV}/c$. However, the S0 and the DWT tunes have similar charged particle densities in the “transverse” region for $p_T > 0.9 \text{ GeV}/c$. This is because the S0 tune has a slightly “softer” charged particle p_T distribution than Tune DWT.

S0 and DWT have very similar energy densities in the “transverse” region, however there are interesting differences in shape: in particular S0 predicts a steeper rise with a flatter plateau at $P_T(\text{chgjet1}) \approx 20 \text{ GeV}/c$ for both $p_T > 0.5 \text{ GeV}/c$ and $p_T > 0.9 \text{ GeV}/c$.

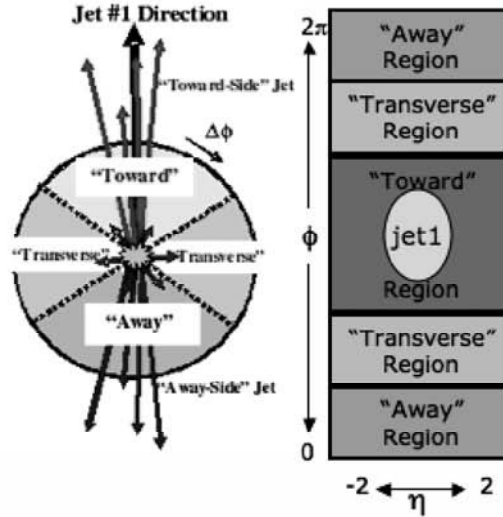


Figure 5.5: Illustration of correlations in azimuthal angle ϕ relative to the direction of the leading charged particle jet (with cone size $R = 0.5$) in the event, chgjet1 . The angle $\Delta\phi = \phi - \phi_{\text{chgjet1}}$ is the relative azimuthal angle between charged particles and the direction of chgjet1 . The “transverse” region is defined by $60^\circ < |\Delta\phi| < 120^\circ$ and $|\eta| < 2$. We examine charged particles in the range $|\eta| < 2$ with $p_T > 0.5 \text{ GeV}/c$ or $p_T > 0.9 \text{ GeV}/c$.

Figures 5.6 and Fig. 5.7 show the QCD Monte-Carlo models predictions for the average density of charged particles, $dN_{\text{chg}}/d\phi d\eta$, and the average charged PT_{sum} density, $dPT_{\text{sum}}/d\phi d\eta$, respectively, in the “transverse” region for $|\eta| < 2$ with $p_T > 0.5 \text{ GeV}/c$ and $p_T > 0.9 \text{ GeV}/c$ versus the transverse momentum of the leading charged particle jet. The charged particle density is constructed by dividing the average number of charged particles per event by the area in η - ϕ space (in this case $4\pi/3$). The charged PT_{sum} density is the average scalar p_T sum of charged particles per event divided by the area in η - ϕ space. Working with densities allows one to compare regions of η - ϕ space with different areas.

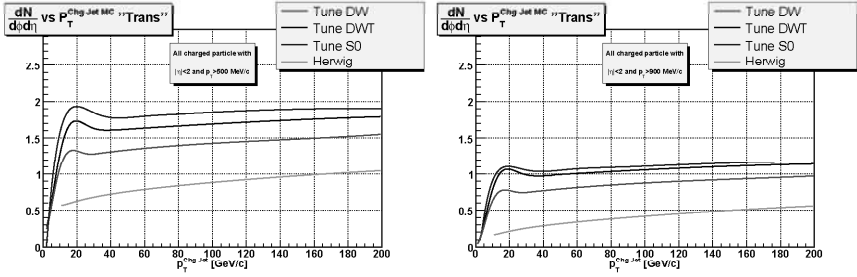


Figure 5.6: QCD Monte-Carlo models predictions for charged particle jet production at 14 TeV. Observables in the “transverse” region. Average density of charged particles, $dN_{chg}/d\phi d\eta$, with $|\eta| < 2$ and $p_T > 0.5$ GeV/c (*left*) or $p_T > 0.9$ GeV/c (*right*) versus the transverse momentum of the leading charged particle jet. The QCD models are HERWIG (without MPI) and three versions of PYTHIA 6.4 (with MPI).

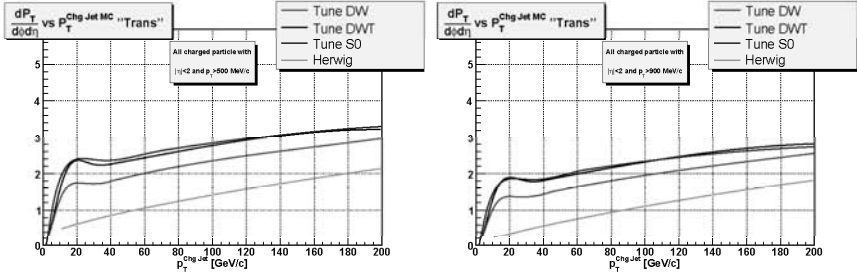


Figure 5.7: QCD Monte-Carlo models predictions for charged particle jet production at 14 TeV. “transverse” region: average charged PT_{sum} density, $dPT_{sum}/d\phi d\eta$, with $|\eta| < 2$ and $p_T > 0.5$ GeV/c (*left*) or $p_T > 0.9$ GeV/c (*right*) versus the transverse momentum of the leading charged particle jet. The QCD models are HERWIG (without MPI) and three versions of PYTHIA 6.4 (with MPI).

Figures 5.8 and Fig. 5.9 show the same quantities, $dN_{chg}/d\phi d\eta$ and PT_{sum} for QCD Monte-Carlo models and superimposed the full simulation results for CMS experiment. The reconstructed points are referred to 10 pb^{-1} of low luminosity operation at LHC, without pile up. The complete analysis is described elsewhere (25). Even with a reduced integrated luminosity, 10 pb^{-1} ,

it is possible to discriminate between different models taking the advantage to reconstruct tracks down to p_T of 500 MeV/c.

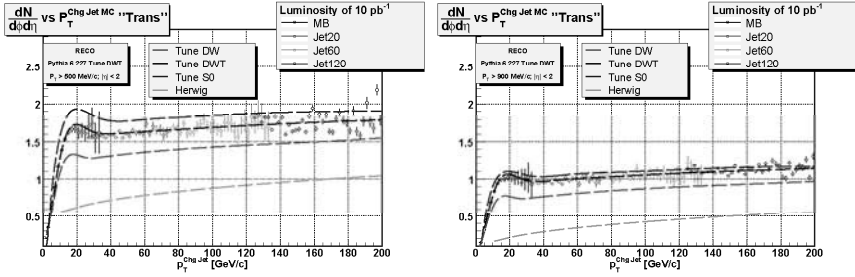


Figure 5.8: QCD Monte-Carlo models predictions for charged particle jet production at 14 TeV. “transverse” region: average charged PT_{sum} density, $dPT_{sum}/d\phi d\eta$, with $|\eta| < 2$ and $p_T > 0.5$ GeV/c (left) or $p_T > 0.9$ GeV/c (right) versus the transverse momentum of the leading charged particle jet. The QCD models are HERWIG (without MPI) and three versions of PYTHIA 6.4 (with MPI).

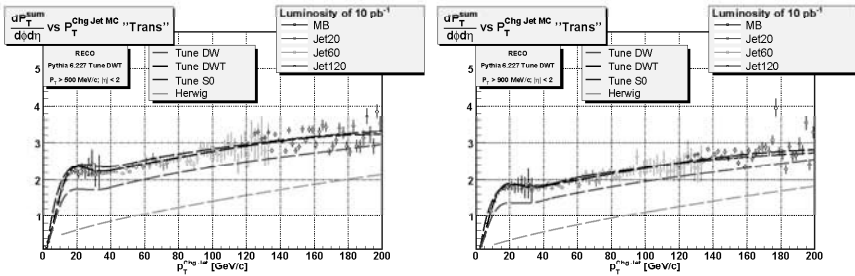


Figure 5.9: QCD Monte-Carlo models predictions for charged particle jet production at 14 TeV. “transverse” region: average charged PT_{sum} density, $dP_T^{sum}/d\phi d\eta$, with $|\eta| < 2$ and $p_T > 0.5$ GeV/c (left) or $p_T > 0.9$ GeV/c (right) versus the transverse momentum of the leading charged particle jet. The QCD models are HERWIG (without MPI) and three versions of PYTHIA 6.4 (with MPI).

5.5 The Direct Observation of Multiple Partonic Interactions

The final goal of the MPI study is to achieve a uniform and coherent description of MPI processes for both high- and the low- P_T regimes. Recent theoretical progress in this field has been reported (26). The cross section for a double high- P_T scattering is parameterized as:

$$\sigma_D = \frac{m\sigma_A\sigma_B}{2\sigma_{eff}}$$

where A and B are 2 different hard scatters, $m=1,2$ for indistinguishable or distinguishable scatterings respectively and σ_{eff} contains the information about the spatial distribution of the partons (27) (28). In this formalism $m\sigma_B/2\sigma_{eff}$ is the probability that an hard scatter B occurs given a process A and this does strongly depend on the geometrical distribution of the partons inside the interacting hadrons. The LHC experiments will perform this study along the lines of the CDF experiments (29) (30)), i.e. studying 3jet+ γ topologies. On top of that the extension to the study of same sign W production (Fig. 5.10) is also foreseen. Here we would like to propose an original study concentrating on the search for perturbative patterns in MB events looking for minijet pair production.

Let's introduce the formalism for the study of MPI in mini-jet production. We re-write the inelastic cross section as the sum of one soft and one hard component.

$$\sigma_{inel} = \sigma_{soft} + \sigma_{hard} \quad (5.2)$$

with σ_{soft} the soft contribution to the inelastic cross section σ_{inel} , the two contributions σ_{soft} and σ_{hard} being defined through the cutoff in the momentum exchanged between partons, p_t^c . Notice that, differently from the case of the inclusive cross section (σ_S), which is divergent for $p_t^c \rightarrow 0$, both σ_{hard} and all exclusive contributions to σ_{hard} , with a given number of parton collisions, are finite in the infrared limit.

A simple relationship links the hard cross section to $\langle N \rangle$, i.e. the average number of partonic interactions:

$$\langle N \rangle \sigma_{hard} = \sigma_S \quad (5.3)$$

While the effective cross section σ_{eff} turns out to be linked to the dispersion $\langle N(N-1) \rangle$:

$$\frac{1}{2} \langle N(N-1) \rangle \sigma_{hard} = \sigma_D \quad (5.4)$$

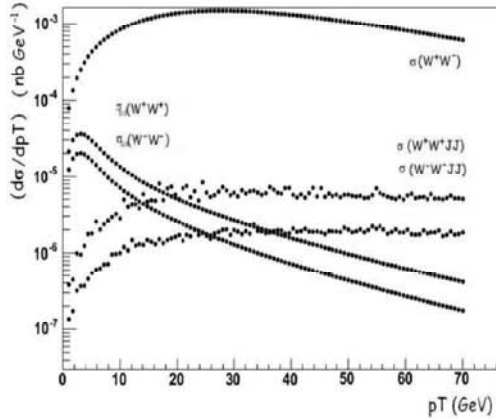


Figure 5.10: differential cross section for same sign W production versus the minimum p_T of the boson pair. Contribution from double parton interactions are superimposed to those arising from single parton interaction processes. W^+W^- cross section is also drawn as reference.

These relationships can be used to express σ_{eff} in terms of the statistical quantities related to the multiplicity of partonic interactions:

$$\langle N(N - 1) \rangle = \langle N \rangle^2 \frac{\sigma_{hard}}{\sigma_{eff}} \tag{5.5}$$

This last equation is particularly relevant from an experimental point of view. Indeed, even with a reduced detector acceptance and detection efficiency, one can always measure the physical observable $\sigma_{hard}/\sigma_{eff}$ that accounts for the probability enhancement of having additional partonic interactions above the scale p_t^c .

We propose to perform this measurement counting the charged mini-jet pairs above a minimal scale p_t^c in MB events. Mini-jets are reconstructed along the lines described in the previous sub-section. First of all the charged jets are p_T -ordered. A pairing criteria is introduced which is based on the maximum difference in azimuth between the charged jets. The pairing algorithm starts from the leading charged jet and associates the first secondary jet in the hierarchy that respects the criteria. The highest p_T of the pair is assumed to be the scale of the corresponding partonic interaction. The paired charged jets are removed from the list and the remnant charged jets are re-processed following

the same steps. One end-up with a list of paired charged jets. N is the number of charged pairs above the scale p_t^c .

Fig. 5.11 shows the difference in azimuth versus the p_T ratio between the first and the second charged jet in the event. Right plot shows the case when both MPI and radiation are switched off to study the sensitivity of the pairing algorithm in a clean hard process. Two cuts have been set to define the pairs: $\Delta\phi > 2.7$ and $p_T \text{ ratio} > 0.25$.

Fig 5.12 reports σ_{eff} for two different pseudorapidity ranges $|\eta| < 5$ (*left*) and $|\eta| < 2.4$ (*right*). As expected σ_{eff} does not depend on the detector acceptance. In the same figures is shown the sensitivity of the pairing algorithm to radiation coming from initial and final state (red points refer to the no-radiation case).

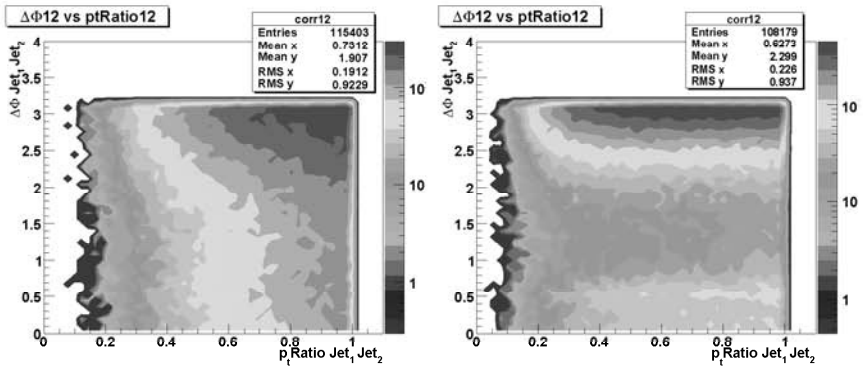


Figure 5.11: Delta azimuth versus the p_T ratio between the first and the second charged jets in MB events at the LHC. Right plot is considered as a cross check for the pairing algorithm when Multiple Parton Interactions and radiation processes are switched off. PYTHIA Tune S0 is considered.

Notice that, while in the result of the simulation the effective cross section does not depend on the acceptance of the detector, one observes same dependence of σ_{eff} on p_t^{min} also after switching off the radiation. One should emphasize that this feature would not show up in the simplest model of multi-parton interactions, where the distribution in the number of collisions, at fixed hadronic impact parameter, is a Poissonian. In this case one would in fact obtain that the effective cross section is constant not only as a function of the acceptance of the calorimeter, but also as a function of the cutoff. A cutoff dependent effective cross section might be produced by a distribution in the number of collisions at fixed impact parameter different from a Poissonian. It

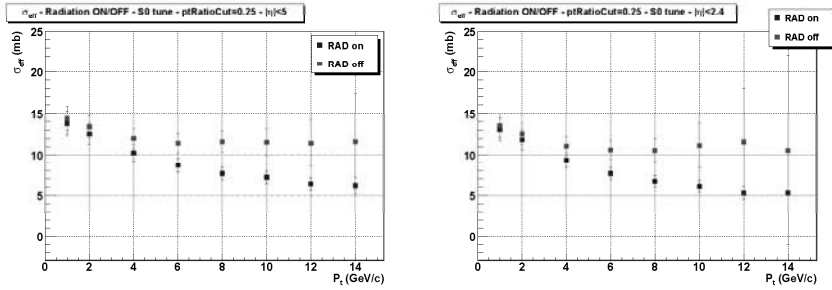


Figure 5.12: Effective cross section in MB events at the LHC quoted for minijet processes in two different pseudorapidity ranges: $|\eta| < 5$ (left) and $|\eta| < 2.4$ (right) with and without radiation processes (blu and red). PYTHIA Tune S0 is considered.

should be remarked that considering a distribution, at fixed impact parameter, different from a Poissonian one introduces correlations in the multiparton distributions additional to the correlation in the transverse parton coordinates, taken into account by the dependence of the average number of multiparton collisions on the impact parameter. Observing a dependence of σ_{eff} on p_t^{min} one would hence provide evidence of further non trivial correlations effects between partons in the hadron structure. To trace back the origin of the dependence of σ_{eff} on p_t^{min} , observed in the simulation, one might notice that, in the simplest uncorrelated Poissonian model, the impact parameter is chosen accordingly with the value of the overlap of the matter distribution of the two hadrons and independently on value of the cutoff p_t^{min} . In Pythia, on the contrary, events are generated through a choice of the impact parameter which is increasingly biased towards smaller values at large p_t . The correlation induced in this way between the impact parameter of the hadronic collisions and the scale of the interaction has the result of decreasing the behavior of σ_{eff} at large p_t^{min} .

References

1. T. Akesson *et al.*, “Double parton scattering in pp collisions at $\sqrt{s} = 63$ GeV”, *Z. Phys. C* **34** (1987) 163.
2. J. Alitti *et al.*, “A Study of multi-jet events at the CERN $\bar{p}p$ collider and a search for double parton scattering”, *Phys. Lett. B* **268** (1991) 145.
3. F. Abe *et al.*, “Study of four jet events and evidence for double parton interactions in $p\bar{p}$ COLLISIONS AT $\sqrt{s} = 1.8$ TEV”, *Phys. Rev. D* **47** (1993) 4857.
4. T. Sjostrand and M. van Zijl, “Multiple Parton-Parton Interactions in an Impact Parameter Picture,” *Phys. Lett. B* **188** (1987) 149.
5. T. Sjostrand, P. Eden, C. Friberg, L. Lonnblad, G. Miu, S. Mrenna and E. Norrbin, “High-energy-physics event generation with PYTHIA 6.1,” *Comput. Phys. Commun.* **135** (2001) 238 [arXiv:hep-ph/0010017].
6. J. M. Butterworth, J. R. Forshaw and M. H. Seymour, “Multiparton interactions in photoproduction at HERA,” *Z. Phys. C* **72** (1996) 637 [arXiv:hep-ph/9601371].
7. T. Gleisberg, S. Hoche, F. Krauss, A. Schalicke, S. Schumann and J. C. Winter, “SHERPA 1.alpha., a proof-of-concept version,” *JHEP* **0402** (2004) 056 [arXiv:hep-ph/0311263].
8. F. W. Bopp, R. Engel and J. Ranft, “Rapidity gaps and the PHOJET Monte Carlo,” arXiv:hep-ph/9803437.
9. G. Corcella *et al.*, “HERWIG 6: An event generator for hadron emission reactions with interfering gluons (including supersymmetric processes),” *JHEP* **0101** (2001) 010 [arXiv:hep-ph/0011363].
10. T. Sjostrand and P. Z. Skands, “Transverse-momentum-ordered showers and interleaved multiple interactions,” *Eur. Phys. J. C* **39** (2005) 129 [arXiv:hep-ph/0408302].
11. P. Nason *et al.*, “Bottom production,” hep-ph/0003142 (2000) 293.
12. G.J. Alner *et al.*, “Scaling of pseudo-rapidity distribution at c.m. energies up to 0.9 TeV”, *Z. Phys. C* **33**, 1 (1986).
13. F. Abe *et al.*, “Pseudo-rapidity distribution of charged particles produced in $p\bar{p}$ interactions at $\sqrt{s} = 630$ GeV and 1800 GeV”, *Phys. Rev. D* **41**, 2330 (1989).

14. G. Gustafson, L. Lonnblad and G. Miu, *Phys. Rev. D* **67** (2003) 034020 [arXiv:hep-ph/0209186].
15. T. Sjostrand, S. Mrenna and P. Skands, *JHEP* **0605** (2006) 026 [arXiv:hep-ph/0603175].
16. G.J. Alner *et al.*, “A general study of proton-antiproton physics at $\sqrt{s} = 546$ GeV”, *Phys. Reports* **154**, 247 (1987).
17. F. Sikler, “Low p(T) hadronic physics with CMS,” arXiv:physics/0702193.
18. A. A. Affolder *et al.* [CDF Collaboration], “Charged jet evolution and the underlying event in proton anti-proton collisions at 1.8-TeV,” *Phys. Rev. D* **65** (2002) 092002.
19. D. Acosta *et al.* [CDF Collaboration], “The underlying event in hard interactions at the Tevatron anti-p p collider,” *Phys. Rev. D* **70** (2004) 072002 [arXiv:hep-ex/0404004].
20. D. Acosta, F. Ambroglini, P. Bartalini, A. De Roeck, L. Fano, R. Field and K. Kotov, “The underlying event at the LHC,”
21. R. Field [CDF Collaboration], “Min-bias and the underlying event in Run 2 at CDF,” *Acta Phys. Polon. B* **36** (2005) 167.
22. F. Abe *et al.* [CDF Collaboration], “Measurement of the Z (p(T)) distribution in anti-p p collisions at $s^{*(1/2)} = 1.8$ -TeV,” *Phys. Rev. Lett.* **67** (1991) 2937.
23. C. M. Buttar, D. Clements, I. Dawson and A. Moraes, “Simulations Of Minimum Bias Events And The Underlying Event, Mc Tuning And Predictions For The Lhc,” *Acta Phys. Polon. B* **35**, 433 (2004).
24. P. Skands and D. Wicke, “Non-perturbative QCD effects and the top mass at the Tevatron,” *Eur. Phys. J. C* **52**, 133 (2007) [arXiv:hep-ph/0703081].
25. F. Ambroglini *et al.*, “Measurement of the Underlying Event in Jet Topologies using Charged Particle and Momentum Densities,” Note in preparation
26. Heavy-quark production in proton-nucleus collisions at the LHC, D. Treleani *et al.*, *Int. J. Mod. Phys. A* **20**: 4462-4468 (2005)
27. N. Paver and D. Treleani, *Nuovo Cim. A* **70** (1982) 215.
28. L. Ametller and D. Treleani, *Int. J. Mod. Phys. A* **3** (1988) 521.

29. Measurement of Double Parton Scattering in $p\bar{p}$ Collisions at $\sqrt{s} = 1.8$ TeV, F. Abe et al., Phys. Rev. Lett. 79, 584 (1997)
30. Measurement of Double Parton Scattering in $p\bar{p}$ Collisions at $\sqrt{s} = 1.8$ TeV, F. Abe et al., Phys. Rev. D 56, 3811 (1997)